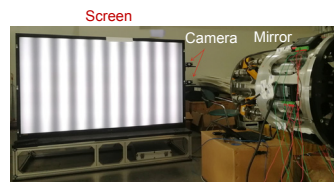


DOI: 10.12086/oee.2020.190435

基于立体相位测量偏折术的 预应力薄镜面形检测

陈贞屹^{1,2}, 赵文川², 张启灿^{1*}, 汉 语², 刘元坤¹



¹ 四川大学电子信息学院, 四川 成都 610065;

² 中国科学院光电技术研究所, 四川 成都 610209

摘要: 应力抛光技术通过在镜面上施加预定载荷, 将包括自由曲面在内的非球面转化为球面进行加工, 对加工镜面的形变进行精准检测是实现高精度应力抛光的关键。利用立体相位测量偏折术对预应力薄镜进行镜面面形和形变检测, 获得被测镜表面的连续相位分布, 结合表面法线唯一性与梯度分布积分, 最终得到被测镜的高度分布和面形。模拟了系统误差成分, 同时采用旋转平均法对系统误差进行标定去除, 保证和提高了测量精度。对一块口径 320 mm, 球面半径 5200 mm 的预应力薄镜面形和变形量进行测量, 静态测量结果与三坐标机测量结果对比, 动态应变测量结果与有限元仿真结果对比, 分别一致吻合, 表明本文方法具备微米级的测量精度, 相比于干涉仪和三坐标机更适用于大面积变化的预应力薄镜检测。

关键词: 光学面形检测; 立体相位测量偏折术; 系统误差; 预应力抛光

中图分类号: TN247; TH741

文献标志码: A

引用格式: 陈贞屹, 赵文川, 张启灿, 等. 基于立体相位测量偏折术的预应力薄镜面形检测[J]. 光电工程, 2020, 47(8): 190435

Shape measurement of stressed mirror based on stereoscopic phase measuring deflectometry

Chen Zhenyi^{1,2}, Zhao Wenchuan², Zhang Qican^{1*}, Han Yu², Liu Yuankun¹

¹School of Electronics and Information Engineering, Sichuan University, Chengdu, Sichuan 610065, China;

²Institute of Optics and Electronics, Chinese Academy of Sciences, Chengdu, Sichuan 610209, China

Abstract: Stressed polishing technology transforms aspheric fabrication into spherical fabrication by applying pre-determined loads on the surface of the mirror. The key to achieve high precision of stressed polishing is to test the surface deformation with high precision. Stereoscopic phase measuring deflectometry was used to test the surface topography and the deformation of stressed mirror. After obtained unwrapped phase distribution, and combined with normal consistency constraint and gradient integral algorithm, the height distribution was finally obtained. Composition of systematic errors were simulated. Also, the errors were calibrated and removed by N-step averaging method in this system, which improved the measuring precision. In this paper, the surface topography and the deformation of a stressed mirror with a diameter of 320 mm, spherical radius of 5200 mm were measured. The measuring results

收稿日期: 2019-07-23; 收到修改稿日期: 2019-10-22

基金项目: 国家自然科学基金资助项目(61675141, 61505216); 中国科学院青年创新促进会资助

作者简介: 陈贞屹(1995-), 男, 硕士研究生, 主要从事光学元件三维形貌测量的研究。E-mail: 13628045693@163.com

通信作者: 张启灿(1974-), 男, 博士, 教授, 主要从事三维传感、动态三维测量等研究。E-mail: zqc@scu.edu.cn

版权所有©2020 中国科学院光电技术研究所

were consistent with the corresponding result of CMM and finite element simulation, indicating that this proposed method is on the level of micron in terms of accuracy and more suitable for the test of stressed mirror compared with interferometer and CMM.

Keywords: optical testing; stereoscopic phase measuring deflectometry; systematic error; stressed mirror polishing

Citation: Chen Z Y, Zhao W C, Zhang Q C, et al. Shape measurement of stressed mirror based on stereoscopic phase measuring deflectometry[J]. *Opto-Electronic Engineering*, 2020, 47(8): 190435

1 引言

拼接镜面主动光学技术在大口径望远镜研制过程中的成功应用，帮助天文望远镜突破了口径限制^[1]。然而随着主镜口径的不断增大，构成主镜所需的离轴子镜数量也呈几何量级增长。为实现离轴子镜的高效率加工，加州大学 Nelson 教授等^[2-3]提出了应力抛光技术，该技术能够将包括自由曲面在内的非球面转化为球面进行加工，与数控子孔径加工技术相比，材料去除效率大幅提高^[4]。

应力抛光技术的关键之一是对镜面变形进行精准测量，现今主要测量手段包括干涉仪和三坐标机。通常，此类被测镜球面曲率半径较大，长达数米，若使用干涉测量^[5]，干涉仪需放在曲率中心处，测量距离也达到数米，空气扰动将大大影响测量结果；另外，预应力薄镜的变形量通常都在微米量级以上，超出了干涉仪的动态范围而无法测量。三坐标机测量属于接触式测量，测头需要与镜面接触，采样密度低，测量速度慢，无法对面形进行实时反馈。

相位测量偏折术(Phase measuring deflectometry, PMD)基于结构光三维检测技术，具有系统简单、成本低、动态范围大、灵敏度高、测量效率高的特点^[6-7]，经过高精度的系统标定与误差校准，可以实现高精度的面形测量。同时，通过条纹的相对变形，可以很精

确地检测到面形的变化，也就是说，该技术可以非常方便容易地测量面形的相对变化，非常适合预应力薄镜的检测需求。本文研究将立体相位测量偏折术运用到预应力薄镜的面形检测中，同时结合旋转平均法消除系统误差影响，实现了对一块口径 320 mm，球面半径 5200 mm 的预应力薄镜初始状态面形和面形变形量的快速测量，结果与三坐标机以及有限元仿真理论影响力函数对比一致。

2 基本原理

测量系统如图 1 所示，由相机、被测镜、显示屏组成。两个相机通过被测镜的反射，拍摄显示屏上依次相移的水平和垂直方向正弦条纹，经过相移条纹的对应相位计算和相位展开后，得到携带了被测镜面形信息的连续相位分布。按照光线可逆原理，假设光线从相机发出，相机每个像素点发出的光线经被测面反射后最终入射到显示屏上。在针孔相机模型下，由连续相位分布可以得到相机每个像素点入射到显示屏上的坐标。

在立体相位测量偏折术中，Camera1 任意像素点 p_1 出射到被测镜上的物点坐标可通过假设来确定。如图 2 所示， c_1, c_2 分别为 Camera1 和 Camera2 的相机光心，实际上情况下， p_1 对应的物点位置应在被测镜表面的 o 点， p_1 发出的光线入射到显示屏上的点为 q_1 ，

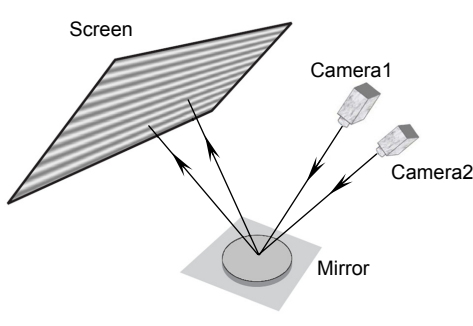


图 1 测量系统示意图

Fig. 1 Schematic diagram of the measurement system

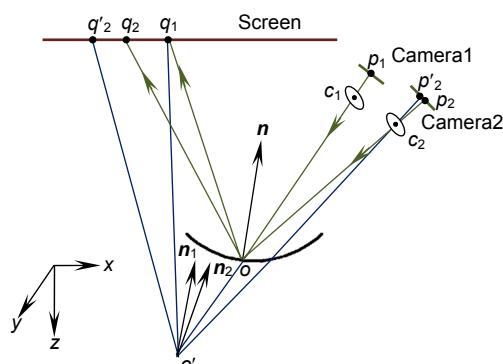


图 2 双目 PMD 原理示意图

Fig. 2 Schematic diagram of stereoscopic PMD

Camera2 对 o 点的成像点为 p_2 , p_2 发出的光线入射到显示屏上的点为 q_2 。现假设 p_1 点对应的物点位置在 o' 处, 则 Camera2 的成像点由 p_2 变为 p'_2 , 经过 o' 点的光线与显示屏的交点由 q_2 变为 q'_2 。由 p_1, o', q_1 和 p'_2, o', q'_2 的坐标可分别算出 Camera1, Camera2 中 o' 点的表面法线 n_1, n_2 。根据法线唯一性原则^[8-9], 如果假设的点 o' 在真实物点 o 处, 则 n_1 应该与 n_2 相等, 否则继续假设物点位置, 反复迭代前述过程, 直到 $n_1=n_2$ 为止, 由此 o 点的坐标便可找到。

理论上对所有点都使用该法线唯一性就可求出整个被测镜的面形和高度, 但由于双目视觉测量精度对噪声比较敏感, 测得精度有限, 计算速度也非常慢^[10]。本文将利用假设点的法线束来获取梯度分布^[10], 结合一个可靠点的准确高度, 通过 Southwell 模型区域波前重构积分^[11-13]得到初始面形分布, 反复迭代此过程得到被测面真实面形^[14]。由于选取的可靠点往往不是被测镜中心点, 导致积分的采样面坐标系与物体坐标系间有一定旋转, 在得到恢复的矢高面形后, 应将面形旋转回物体坐标系。

从光强中提取的相位信息除了被测反射镜的高度调制相位, 还有系统误差, 因此最后恢复的反射镜面形也包含了系统误差。这些误差来自于条纹屏平面性、相机噪声、计算积分时误差扩散和系统标定引入的误差等^[15], 其中系统标定的误差是主要影响因素^[16]。如何去除这些系统误差将取决于其组成成份。为了检验和分析此系统中标定不准确带来的系统误差成份, 根据标定的系统位置参数建立系统模型^[17], 并模拟了系统误差。图 3 为标定误差较大时的系统误差分布, 表 1 为系统误差的 Zernike 多项式分解。表 1 的结果证明

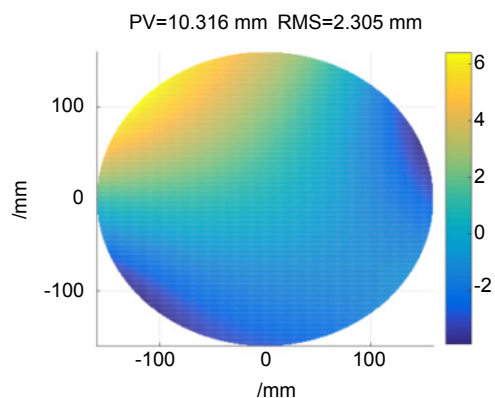


图 3 模拟系统误差分布

Fig. 3 Simulation of the systematic error distribution

了 PMD 中系统误差主要是低阶非旋转对称部分^[18]。因此, 本文采用旋转平均法^[19-21]来标定和去除系统误差, 有效保证和提升测量精度。

3 实验

实验装置由 2 个 CCD 相机 (PointGrey, GS3-U3-28S5M-C, 分辨率为 1920 pixels×1440 pixels, 像素尺寸为 4.54 μm)、一个 80 寸(1 寸=2.54 cm)液晶显示屏(Sharp, LCD-80X818A, 分辨率为 3840 pixels×2160 pixels)、被测弯月型薄镜及其支撑装置和计算机构成, 如图 4 所示。所使用的 2 个 CCD 相机分上下放置在显示器同一侧, 取下方相机为主相机。被测预应力薄镜系统如图 5(a)所示, 口径为 320 mm, 其球面半径为 5200 mm, 被固定在一个转台上, 可灵活旋转。薄镜后表面中心有一个固定支撑点, 外沿均匀分布 6 个机电式力促动器(分别记为 1,2,3,4,5,6 号电机), 如图 5(b) 所示。被测薄镜位置距离显示屏约 2000 mm 左右。

测量前首先进行系统标定, 先标定 2 个相机的内参^[22-23]并计算彼此相对位置^[24], 再用标准靶面当作反射镜标定屏幕与主相机的相对位置^[24-25]。图 6 是系统

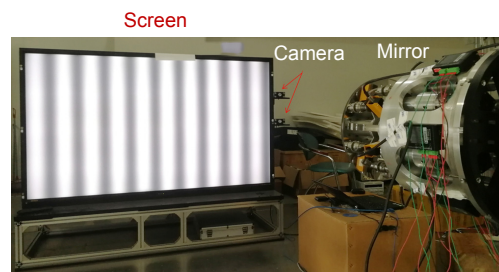


图 4 测量装置图

Fig. 4 Measuring device setup

表 1 系统误差的 Zernike 系数

Table 1 Zernike polynomial coefficient for systematic error

n	m	Coefficient	n	m	Coefficient
0	0	0.1126	3	1	9.5479E-04
1	-1	-1.0312	3	3	0.0026
1	1	1.6773	4	-4	0.2042
2	-2	-1.1339	4	-2	1.3475E-04
2	0	-0.1915	4	0	1.4586E-04
2	2	0.2706	4	2	1.4092E-04
3	-3	1.6649E-04	4	4	-4.8459E-04
3	-1	-1.3508E-04			

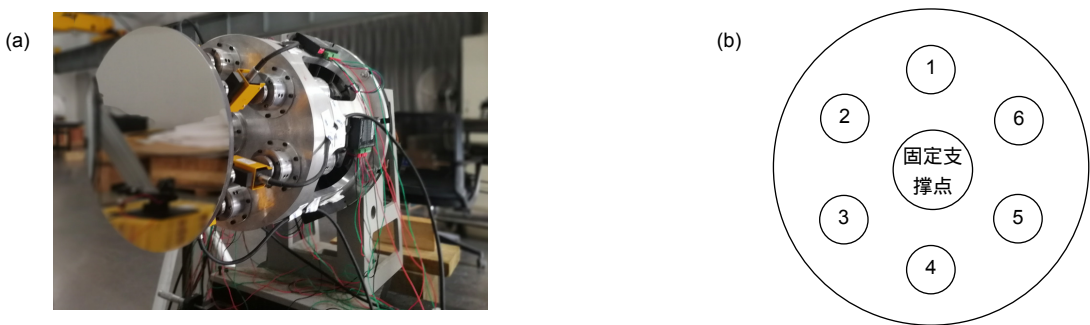


图 5 被测预应力薄镜。(a) 薄镜旋转支撑结构侧视图; (b) 薄镜背面支撑点位置分布示意图

Fig. 5 Stressed mirror under test. (a) Side view of the rotating support structure;
(b) Schematic diagram of support points distribution on the back of the mirror

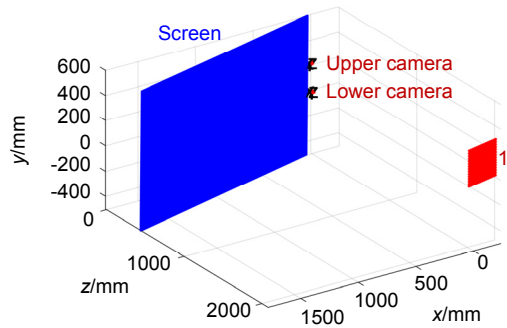


图 6 系统位置参数标定结果示意图

Fig. 6 Schematic diagram of system pose parameter in calibration results

位置参数标定结果示意图，1号靶面即为标定相机与屏幕关系的标定靶，标定双目系统的靶面位置在图中已省略。

3.1 初始状态面形测量

测量中采用了时间相位展开算法^[26-27]进行相位计算，拍摄变形条纹时在显示器上分别用不同频率、水平和竖直不同方向上的各 3 组条纹图相移 4 次，拍摄

耗时约 40 s，图 7 为上下相机拍摄的一帧图像。使用了旋转平均法进行系统误差标定，每隔 60° 转动薄镜一次，一共转动 6 次完成一周 360° 的测量，在每个旋转位置上分别测量 3 次，求平均值作为该旋转度数位置下的测量面形，6 个度数下测量的矢高如图 8 所示。

图 9 为旋转平均法求出的系统误差，图 10 为去系统误差、平移、倾斜和旋转对称项后的镜面面形，其 PV=4.53 μm，RMS=0.754 μm。图 11 为三坐标机的测量数据除去平移、倾斜、旋转对称部分后的面形误差分布(PV=7.879 μm, RMS=1.163 μm)。对比两图可以看出，本文方法的测量结果与三坐标机检测结果分布大体一致。需要说明的是，在进行三坐标测量时，预应力薄镜镜面竖直向上，而在本系统测量中，预应力薄镜镜面是水平方向。

3.2 变形量测量

预应力薄镜背面的力促动电机可对镜体施加双向载荷，除了每个电机独立工作对镜面产生变形以外，6 个电机还可以同时施加不同的校正力，产生球差、像散、慧差、三叶草像差。现将 6 个力促动电机分别单

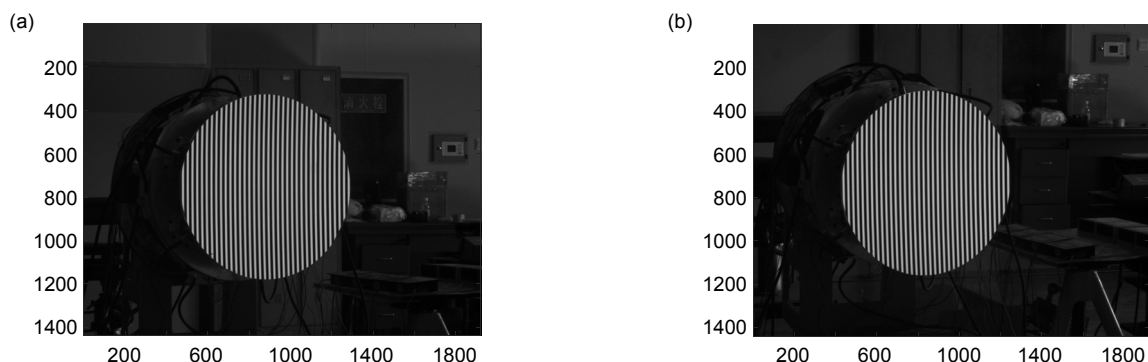


图 7 显示竖直方向相移条纹时拍摄的条纹图。(a) 下相机图拍摄; (b) 上相机图拍摄

Fig. 7 Fringe image in the vertical direction. (a) By lower camera; (b) By upper camera

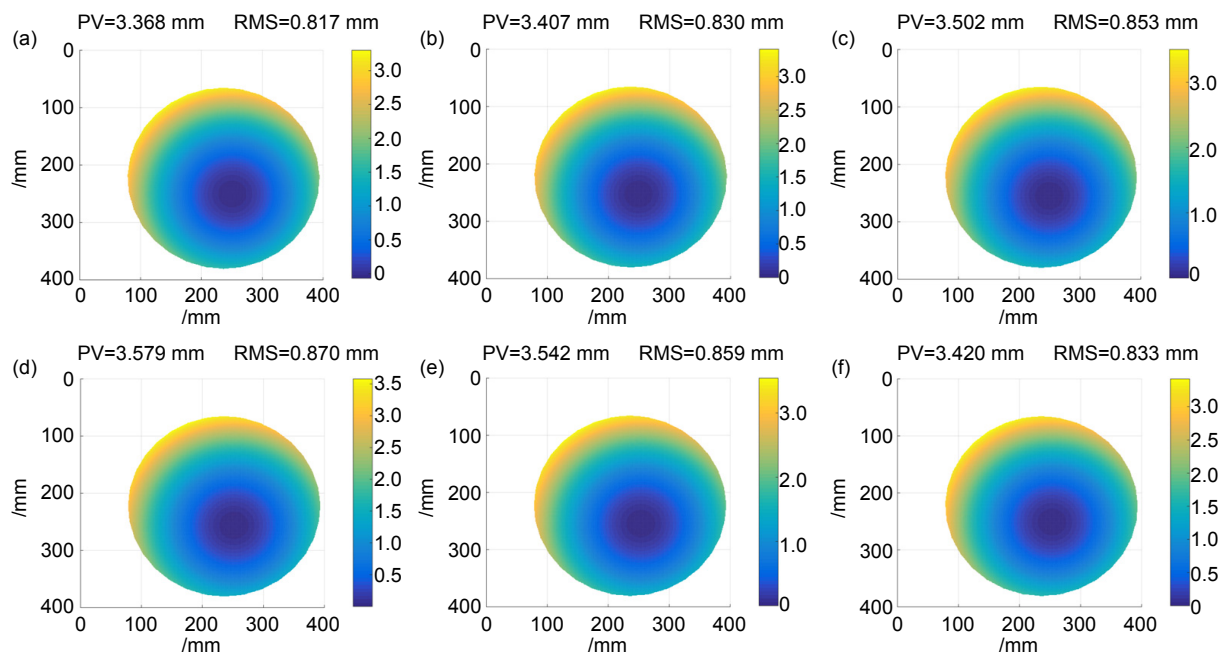


图 8 6 个旋转角度下的薄镜表面矢高测量结果。(a) 0°; (b) 60°; (c) 120°; (d) 180°; (e) 240°; (f) 300°
Fig. 8 Heights measuring results of stressed mirrors at 6 rotation angles. (a) 0°; (b) 60°; (c) 120°; (d) 180°; (e) 240°; (f) 300°

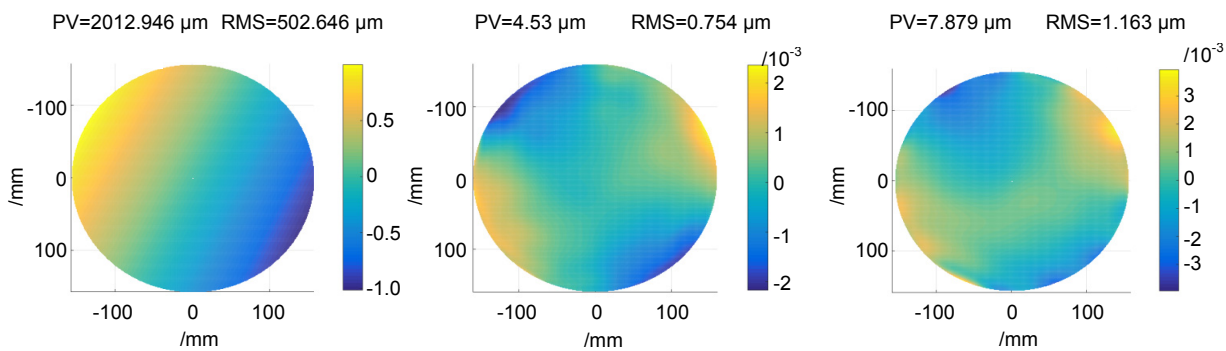


图 9 系统误差分布
Fig. 9 Systematic error distribution

图 10 去除系统误差后的镜面面形
Fig. 10 Mirror shape after removing systematic errors

图 11 三坐标机测量的薄镜面形结果
Fig. 11 Results of stressed mirror measured by CMM

独施加 5 N 的力向外顶，通过对变形前后两次面形测量结果相减，得到各电机单独加力后的镜面变形量。

图 12 分别是 ANSYS 仿真的 1~6 号促动器施加 5 N 外力的理论影响力函数分布，图 13 为实测结果。图 14 为理论分析与实际测量的 PV、RMS 折线图。

从图中可以看出，理论上单个电机施加 5 N 的力能造成镜面约 1.68 μm 的变形量，与实际测量结果一致，幅度和分布也一致。各电机分布中心处的低点是因为镜面后表面中心为固定支撑点时，边缘促动电机外顶造成的；加力电机另一边的镜面突起也是由于中心被固定后，另一边被作用点一同带起。

接着对预应力薄镜的像差变形进行了测量，四种像差的理论目标校正函数如图 15 所示，对应变形后的

检测结果如图 16 所示，表 2 为理论目标校正函数与实际变形检测结果的 PV、RMS 对比。图表展示的结果表明，4 种像差对应薄镜变形的本文检测结果和相应的目标校正函数是一致的。

4 结 论

本文充分利用偏折术测量速度快、动态范围大和灵敏度高的特点，采用立体相位测量偏折术，对预应力薄镜的初始面形和应变量进行了检测。与三坐标机检测方法相比，该方法结构简单，可以一次完成非接触全场测量，可以对面形变形进行快速反馈。与干涉方法相比，该方法有更大的测量动态范围，受环境振动和气流影响更小。这些特点使该方法非常适用于大

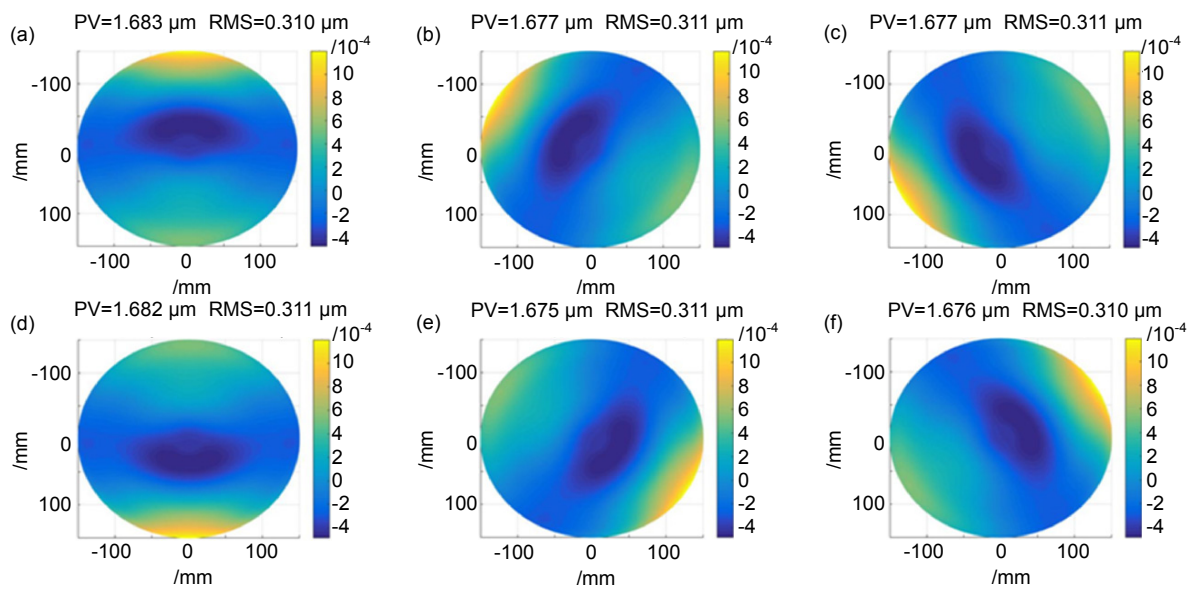


图 12 各个促动电机单独施力的理论影响力函数。 (a) 1 号; (b) 2 号; (c) 3 号; (d) 4 号; (e) 5 号; (f) 6 号
Fig. 12 Theoretical influence function of each actuating motor. (a) No. 1; (b) No. 2; (c) No. 3; (d) No. 4; (e) No. 5; (f) No. 6

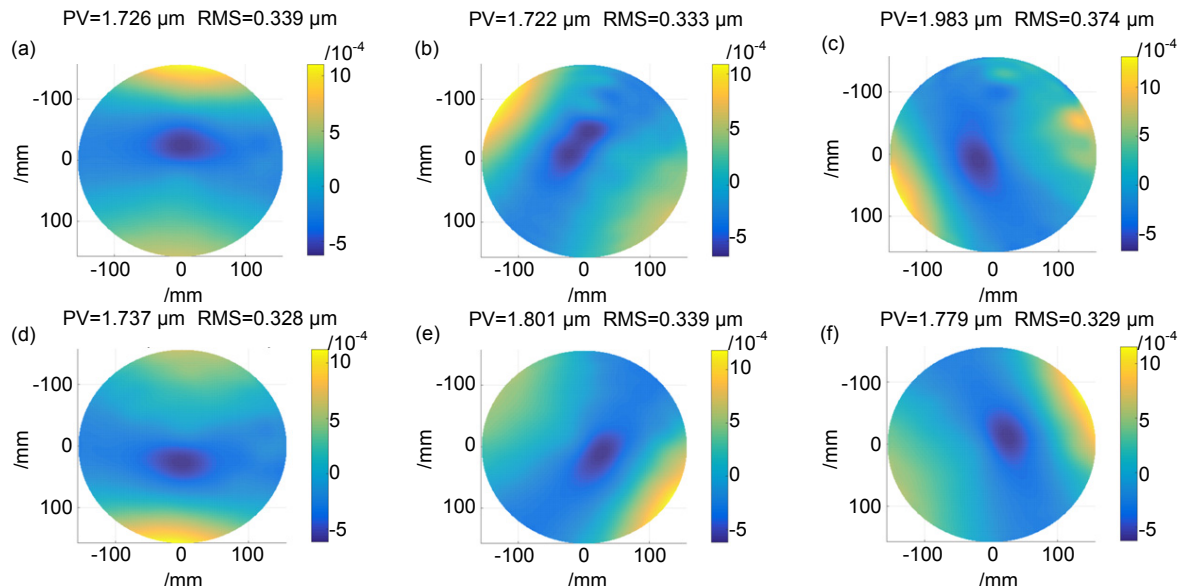


图 13 各个促动电机单独施力的变形量测量结果。 (a) 1 号; (b) 2 号; (c) 3 号; (d) 4 号; (e) 5 号; (f) 6 号
Fig. 13 Deformation measurement results of each actuating motor. (a) No. 1; (b) No. 2; (c) No. 3; (d) No. 4; (e) No. 5; (f) No. 6

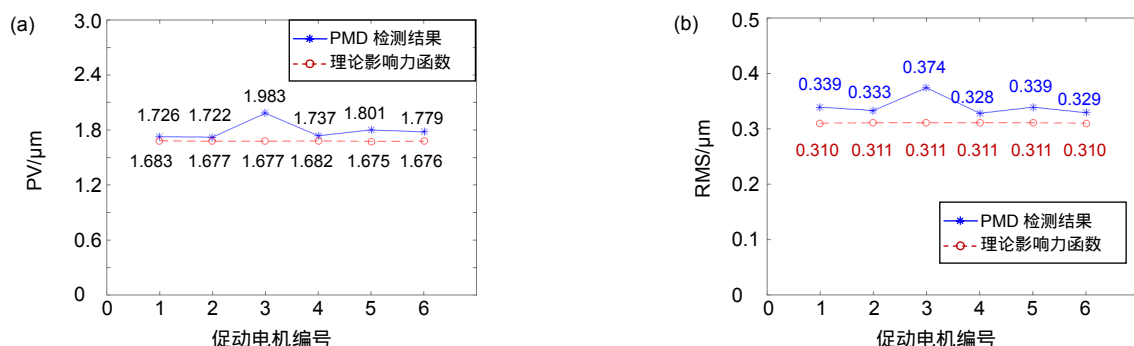


图 14 电机理论变形与实测变形对比。 (a) PV; (b) RMS
Fig. 14 Comparison of theoretical deformation and measuring deformation of each actuating motor. (a) PV; (b) RMS

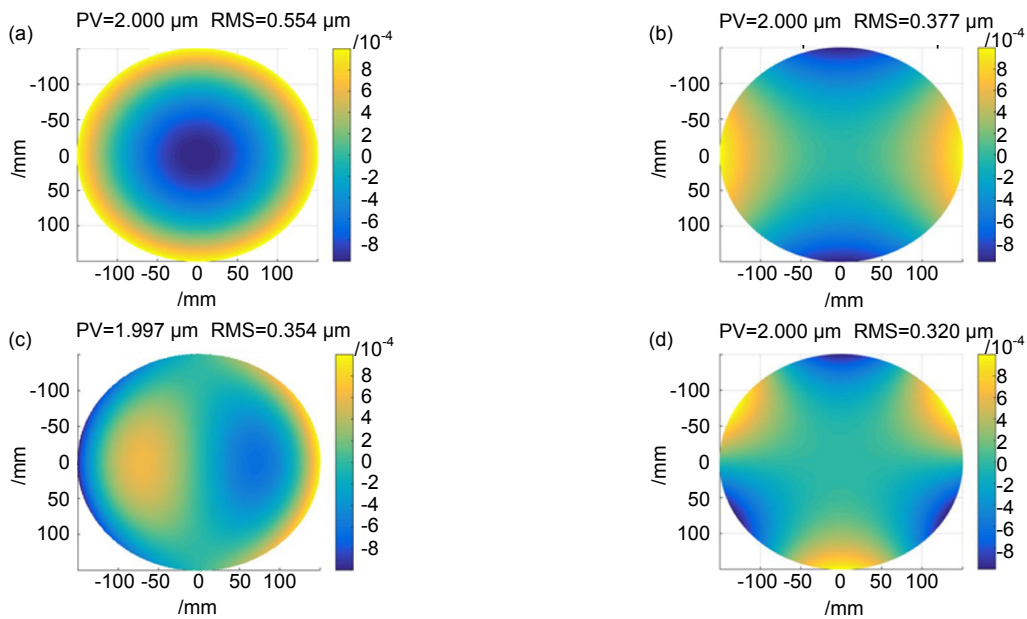


图 15 4 种像差的理论目标校正函数。(a) 球差; (b) 像散; (c) 慧差; (d) 三叶草像差
Fig. 15 Theoretical target correction functions of 4 aberrations. (a) Spherical; (b) Astigmatism; (c) Coma; (d) Trefoil

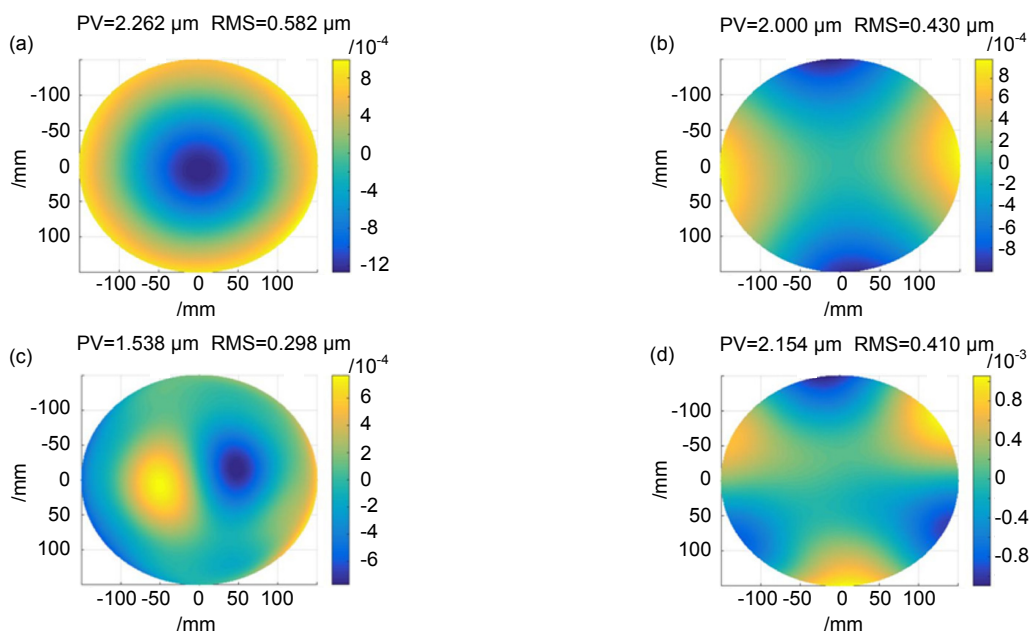


图 16 4 种像差的变形量实测结果。(a) 球差; (b) 像散; (c) 慧差; (d) 三叶草像差
Fig. 16 Deformation measurement results of 4 aberrations. (a) Spherical; (b) Astigmatism; (c) Coma; (d) Trefoil

表 2 像差理论值与实际测量值对比

Table 2 Comparison between theoretical aberration and measured aberration

Aberrations		Spherical	Astigmatism	Coma	Trefoil
PV/μm	Correction function	2.000	2.000	1.997	2.000
	Measuring results	2.262	2.000	1.538	2.154
RMS/μm	Correction function	0.554	0.377	0.354	0.320
	Measuring results	0.582	0.430	0.298	0.410

口径、大变形量的自由面应力薄镜检测。文中模拟了系统误差成分，并通过旋转平均去除系统误差，保证和提高了检测精度。本文检测结果与三坐标机检测结果的细微差别主要是被测镜体放置方式的不同，导致重力影响的不同而引起的。实验表明，本文方法的检测结果与三坐标机测量结果，以及促动器的理论目标函数结果相一致。

本文拓展了相位测量偏折术的应用领域，将其应用于预应力薄面形检测中，下一步可对镜面面形进行实时监测，对力促动器的性能和效果进行实时测量反馈，提高校正的动态能力。另外，在后续工作中，可在标定显示屏与主相机位置关系时使用平面性更好的标准反射镜，或者用三坐标机先对显示屏的平面性进行检测，消除非平面性引入的误差，以进一步提高测量精度。

参考文献

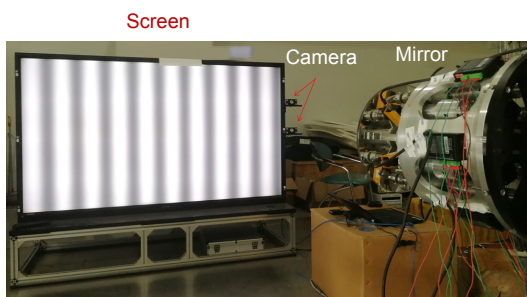
- [1] Li X N, Jiang Z B, Gong X F, et al. Stressed mirror annular polishing for scale-down TMT primary segments[J]. *Proceedings of SPIE*, 2016, **9912**: 99120A.
- [2] Lubliner J, Nelson J E. Stressed mirror polishing. 1: A technique for producing nonaxisymmetric mirrors[J]. *Applied Optics*, 1980, **19**(14): 2332–2340.
- [3] Nelson J E, Gabor G, Hunt L K, et al. Stressed mirror polishing. 2: fabrication of an off-axis section of a paraboloid[J]. *Applied Optics*, 1980, **19**(14): 2341–2352.
- [4] Li X N, Zhang H Y, Cui X Q, et al. Study on stressed mirror polishing with continuous polishing machine for large aperture off-axis aspheric mirror[J]. *Acta Astronomica Sinica*, 2012, **53**(2): 161–170.
李新南, 章海鹰, 崔向群, 等. 大口径离轴非球面镜预应力环抛光法研究[J]. 天文学报, 2012, **53**(2): 161–170.
- [5] Valente M, Lewis B, Melena N, et al. Advanced surface metrology for meter-class optics[J]. *Proceedings of SPIE*, 2013, **8838**: 88380F.
- [6] Huang L, Idir M, Zuo C, et al. Review of phase measuring deflectometry[J]. *Optics and Lasers in Engineering*, 2018, **107**: 247–257.
- [7] Zhao W C, Zhou M, Liu H T, et al. The off-axis aspheric mirror testing based on the fringe reflection technique[J]. *Opto-Electronic Engineering*, 2018, **45**(7): 170663.
赵文川, 周敏, 刘海涛, 等. 离轴非球面的条纹反射检测技术[J]. 光电工程, 2018, **45**(7): 170663.
- [8] Liu F M, Lin J R, Sun Y B, et al. Calibration method for stereo phase measuring deflectometry system[J]. *Laser & Optoelectronics Progress*, 2020, **57**(5): 051202.
刘方明, 林嘉睿, 孙岩标, 等. 一种立体相位偏折测量系统标定方法[J]. 激光与光电子学进展, 2020, **57**(5): 051202.
- [9] Knauer M C, Kaminski J, Häusler G. Phase measuring deflectometry: a new approach to measure specular free-form surfaces[J]. *Proceedings of SPIE*, 2004, **5457**: 366–376.
- [10] 毛心洁. 基于双目立体视觉的镜面物体三维轮廓测试技术[D]. 南京: 南京理工大学, 2017: 48–49.
- [11] Southwell W H. Wave-front estimation from wave-front slope measurements[J]. *Journal of the Optical Society of America*, 1980, **70**(8): 998–1006.
- [12] Zhu Y J, Zhu L X, Zhong J P, et al. Integration algorithm in three-dimensional plane Shape measuring by fringe reflection[J]. *Acta Photonica Sinica*, 2018, **47**(11): 110–119.
朱勇建, 朱立新, 钟建平, 等. 条纹反射法测量三维面形中的积分算法[J]. 光子学报, 2018, **47**(11): 110–119.
- [13] Yi J Y. Study on mobile phone shell inside and outside surface quality inspection based on fringe projection and fringe reflection technologies[D]. Chengdu: University of Electronic Science and Technology of China, 2016: 41–43.
易京亚. 基于条纹投影和条纹反射的手机壳内外表面质量检测方法[D]. 成都: 电子科技大学, 2016: 41–43.
- [14] Zhao W C, Graves L R, Huang R, et al. Iterative surface construction for blind deflectometry[J]. *Proceedings of SPIE*, 2016, **9684**: 96843X.
- [15] Zhao W C, Su X Y, Liu Y K, et al. Testing an aspheric mirror based on phase measuring deflectometry[J]. *Chinese Journal of Lasers*, 2010, **37**(5): 1338–1341.
赵文川, 苏显渝, 刘元坤, 等. 基于相位偏折术的非球面镜检测方法[J]. 中国激光, 2010, **37**(5): 1338–1341.
- [16] Faber C, Olesch E, Krobot R, et al. Deflectometry challenges interferometry: the competition gets tougher![J]. *Proceedings of SPIE*, 2012, **8493**: 84930R.
- [17] Korsch D, Hunter W R. *Reflective optics*[M]. Academic Press, 1991.
- [18] Su P, Khreishi M, Huang R, et al. Precision aspheric optics testing with SCOTS: a deflectometry approach[J]. *Proceedings of SPIE*, 2013, **8788**: 87881E.
- [19] Song W H, Wu F, Hou X. Method to test rotationally asymmetric surface deviation with high accuracy[J]. *Applied Optics*, 2012, **51**(22): 5567–5572.
- [20] Song W, Wu F, Hou X, et al. Absolute calibration of a spherical reference surface for a Fizeau interferometer with the shift-rotation method of iterative algorithm[J]. *Optical Engineering*, 2013, **52**(3): 033601.
- [21] Yang P, Wu F, Hou X. Simulation analysis of absolute measurement for rotationally asymmetric surface error[J]. *Opto-Electronic Engineering*, 2011, **38**(1): 93–97, 102.
杨鹏, 伍凡, 侯溪. 旋转非对称项面形误差绝对检测的仿真分析[J]. 光电工程, 2011, **38**(1): 93–97, 102.
- [22] Zhang Z. A flexible new technique for camera calibration[J]. *IEEE Transactions on Pattern Analysis and Machine Intelligence*, 2000, **22**(11): 1330–1334.
- [23] Gai Q Y. Optimization of stereo matching in 3D reconstruction based on binocular vision[J]. *Journal of Physics: Conference Series*, 2018, **960**: 012029.
- [24] Liu Y K, Su X Y. Camera calibration with planar crossed fringe patterns[J]. *Optik*, 2012, **123**(2): 171–175.
- [25] Zhou T, Chen K, Wei H Y, et al. Improved system calibration for specular surface measurement by using reflections from a plane mirror[J]. *Applied Optics*, 2016, **55**(25): 7018–7028.
- [26] Saldner H O, Huntley J M. Temporal phase unwrapping: application to surface profiling of discontinuous objects[J]. *Applied Optics*, 1997, **36**(13): 2770–2775.
- [27] Zhao W J, Chen W J, Su X Y. The comparison of several time phase unwrapping methods[J]. *Journal of Sichuan University (Natural Science Edition)*, 2016, **53**(1): 110–117.
赵文静, 陈文静, 苏显渝. 几种时间相位展开方法的比较[J]. 四川大学学报(自然科学版), 2016, **53**(1): 110–117.

Shape measurement of stressed mirror based on stereoscopic phase measuring deflectometry

Chen Zhenyi^{1,2}, Zhao Wenchuan², Zhang Qican^{1*}, Han Yu², Liu Yuankun¹

¹School of Electronics and Information Engineering, Sichuan University, Chengdu, Sichuan 610065, China;

²Institute of Optics and Electronics, Chinese Academy of Sciences, Chengdu, Sichuan 610209, China



Measuring device setup

Overview: Stressed polishing technology was firstly proposed by Jerry E.Nelson in 1980, considered as an effective method of aspheric fabrication. According to the calculated results of elastic mechanics, this method exerts an external force on the mirror to form a deformation which opposite to the desired deformation from spherical surface to off-axis aspheric surface. Under the state of deformation, the mirror is polished into sphere surface. After removing the external force, the required off-axis aspheric surface can be obtained. Because aspheric fabrication is converted to spherical fabrication, tools with large diameter can be used and efficiency is greatly improved.

The key to achieve high precision of stressed polishing is to test the deformation of mirror with high precision. However, the main methods of surface measurement nowadays are interferometer and CMM. If interferometer is used, its dynamic range can only support the detection below micron deformation. If CMM is used, probe may scratch the mirror surface, and the detection tempo is very slow. Furthermore, interferometer and CMM are both expensive and complex equipments.

So, aimed at stressed polishing above micron deformation, stereoscopic phase measuring deflectometry was used to test its surface topography and deformation. It is low cost and convenient technique and only screen, camera, and computer were needed when implemented. More importantly, characteristics such as high dynamic range, full-field three-dimensional measurement and excellent performance in medium and high frequency were brought in, which are very suitable for the test of stressed mirror.

When measuring, firstly calculating the unwrapped phase distribution through CCD cameras, then calculating the height of a specific point on the measured surface using normal consistency constraint, and finally the full-field height distribution was obtained by Southwell gradient integral algorithm. To improve the measuring accuracy, composition of systematic errors were simulated, proved that it mainly includes low-order non-rotational symmetry items. According to simulating results, errors were calibrated and removed by N-step averaging method to get a absolute surface topography.

In this paper, the absolute surface topography and the deformation of a stressed mirror with a diameter of 320 mm, spherical radius of 5200 mm were measured. The measuring results were consistent with the corresponding result of CMM and finite element simulation, indicating that this proposed method is on the level of micron in terms of accuracy and more suitable for the test of stressed mirror compared with interferometer and CMM.

Citation: Chen Z Y, Zhao W C, Zhang Q C, et al. Shape measurement of stressed mirror based on stereoscopic phase measuring deflectometry[J]. *Opto-Electronic Engineering*, 2020, **47**(8): 190435

Supported by National Natural Science Foundation of China (61675141, 61505216) and The Youth Innovation Promotion Association, Chinese Academy of Sciences

* E-mail: zqc@scu.edu.cn